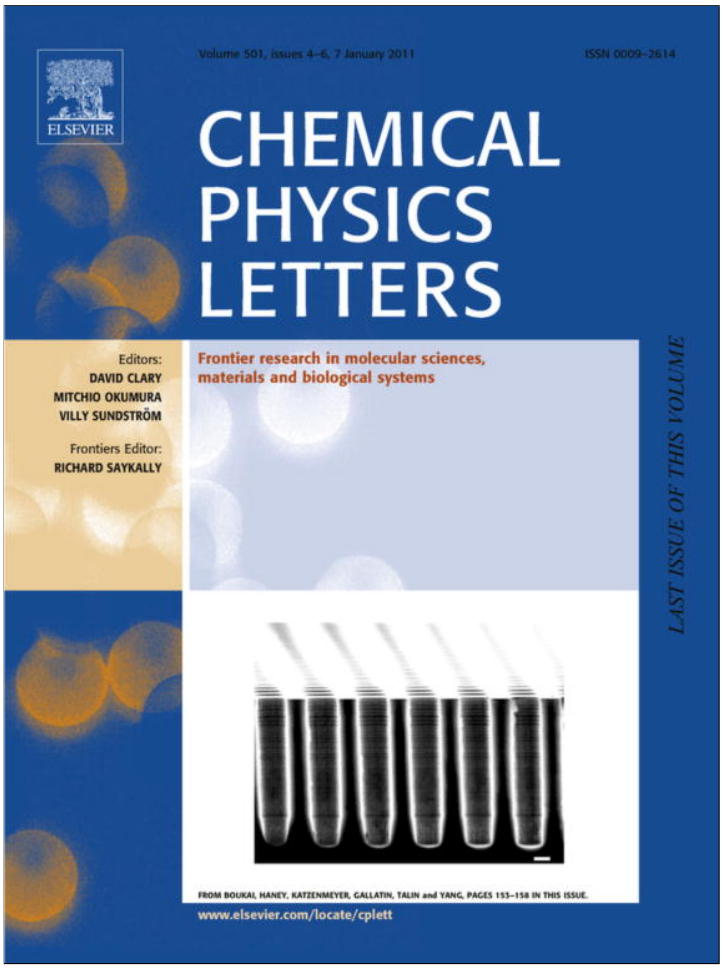

Chemical Physics Letters 501 (2011) 423–426

Contents lists available at ScienceDirect

Chemical Physics Letters

journal homepage: www.elsevier.com/locate/cplett

Carbon nanotube as a gramicidin analogue

Tamsyn A. Hilder *, Shin-Ho Chung

Computational Biophysics Group, Research School of Biology, Australian National University, ACT 0200, Australia

ARTICLE INFO

Article history:
Received 15 October 2010
In final form 10 November 2010
Available online 13 November 2010

ABSTRACT

We have designed a carbon nanotube that is selectively permeable to monovalent cations, binds divalent cations and rejects anions. The nanotubes, with an effective radius of 4.53 Å and length of 36 Å, are terminated with hydrogen atoms and are exohydrogenated in two regions near the entrance and exit. Using molecular and stochastic dynamics simulations we examine the free energy, current–voltage–concentration profiles and ion binding sites. The characteristics of this channel are comparable to the antibiotic gramicidin-A, but the potassium current is six times larger. At 40 mM calcium concentration the current is reduced from 26 pA to 4 pA due to a calcium ion binding at the channel entrance.

1. Introduction

There is ever-increasing interest in designing and fabricating nanotubes that replicate some of the functions of biological ion channels. These synthetic nanotubes have numerous theoretical and practical interests. Studies of these nanotubes may help to improve our understanding of biological ion channels, and could lead to the development of new pharmaceutical products, efficient desalination devices and ultra-sensitive biosensors.

To date, researchers have successfully designed nanotubes made from various materials, such as carbon, that selectively allow water molecules to move across while rejecting all charged particles [1–4]. These nanotubes display substantially faster water conduction than through the biological water channel and reverse osmosis membranes currently being used commercially [3,4]. Furthermore, nanotubes which are selective to either anions or cations have also been designed [5–9]. Hilder et al. [5] design a chloride-selective carbon nanotube (CNT) with conductance four times larger than through the ClC-1 channel and almost twice that of GABA$_A$. Although nanotubes cannot mimic all of the subtle tasks carried out by biological ion channels, several of their features can be fruitfully exploited. Specifically, their length can be tailored to match the thickness of a bilayer [10]; various molecules can be attached to their surface [11] to target specific cells [12] or increase solubility [13]; and they can be made to insert into lipid bilayers [14]. Recently, Lee et al. [15] successfully fabricated single-wall carbon nanotube ion channels 1.5 nm in diameter with negatively charged ends that are capable of selectively conducting protons. By subsequent blocking of larger cations they demonstrate the possibility of a single-ion detection device.

Using the same method as our previous work [5] we investigate a CNT which is specifically designed to broadly mimic some of the conductance properties of gramicidin-A. Gramicidin-A is a polypeptide consisting of 15 amino acid residues, and was one of the first antibiotics isolated and used clinically [16]. As such, it has been the main focus of theoretical investigations for a long time [17]. It forms a cylindrical channel across the bacteria cell membrane and selectively conducts monovalent cations, binds divalent cations and rejects anions [18]. Consequently, the potential across the cell membrane is destroyed, causing the bacteria to become unviable. In a similar manner, a cation-selective nanotube may act to kill bacteria cells or may be made to selectively embed in other target cells. Unfortunately, the insolubility of gramicidin limits its widespread use. In contrast, nanotubes can be made soluble [11].

2. Computational methods

Using molecular dynamics (MD) and distributional molecular dynamics (DMD) [19] simulations we examine a (9,9) single-walled CNT with an effective radius of 4.53 Å and length of 36 Å embedded in a lipid bilayer separating two reservoirs. The nanotube is constructed from a hexagonal array of carbon atoms rolled up to form a cylindrical, hollow tube. Carbon nanotubes spontaneously insert and align across the lipid bilayer once hydrophilic residues, such as hydrogen, are attached at their ends [14]. Therefore, the nanotube is terminated with hydrogen atoms with a partial charge [20] of 0.115 e, and a charge of −0.115 e on the carbon atoms directly bonded to these hydrogens. It is now possible to stably hydrogenate CNTs [21] and site-selectively functionalize their outside surface [22]. However, density functional calculations reveal that not every carbon atom may be bonded to hydrogen, as full coverage is energetically unfavourable [23,24]. Accordingly, the exohydrogenated (outside surface hydrogenation) regions in

* Corresponding author.
E-mail address: tamsyn.hilder@anu.edu.au (T.A. Hilder).

0009-2614/$ - see front matter © 2010 Elsevier B.V. All rights reserved.
doi:10.1016/j.cplett.2010.11.034

our model are partially hydrated (30% coverage). The two hydrated regions, shown in blue in Figure 1A, are from $z = -15.4$ to -12.9 Å and from $z = 12.9$ to 15.4 Å.

We first carry out MD simulations conducted using NAMD [25], visualized with VMD [26], using the CHARMM27 force field [27,28] and TIP3P water model. The MD domain consisted of the functionalized carbon nanotube embedded in a lipid bilayer separated by two reservoirs. The system was replicated in all three dimensions and particle mesh Ewald electrostatics was used. The simulation box was approximately $54 \times 54 \times 97$ Å^3, and contained 4727 water molecules and either 1 potassium, 1 chloride or 1 calcium ion. The center of mass of the nanotube was constrained to allow for tilting of the nanotube, and the nanotube axis was used as the reaction coordinate to measure ion trajectories. No constraints were applied to the lipid bilayer. The three-dimensional potential of mean force (PMF) or free energy was constructed using umbrella sampling at an ionic concentration of 0 mM to avoid double-counting of the ion–ion interactions in subsequent DMD simulations, in which the ion–ion interactions are explicitly dealt with using macroscopic electrostatics [5].

As a result of including only the ion of interest in our simulations, the system will have a non-neutral charge. With particle-mesh Ewald electrostatics, this will result in a uniform neutralizing plasma [29,30]. In other words, a homogeneous neutralizing background charge is implicitly applied to the entire simulation space to avoid the divergence of the Ewald sum and to neutralize the system [29,30]. Although the background charge will alter the free energy profile, its effect can be shown to be negligible for a non-neutral charge of 2 e. The offset of the electrostatic free energy can be determined from [30]

$$\Delta\Delta G_{el}^{ion} \approx -2.837297 \frac{q^2}{8\pi\epsilon_0\epsilon_s L} \tag{1}$$

and in our model is estimated to range from -0.14 kT for potassium to -0.58 kT for a calcium ion, where q is the ionic charge, ϵ_0 is the permittivity of free space, ϵ_s is the solvent permittivity, and L is the unit cell length. To investigate the effect of non-neutral charge we also constructed the free energy profile for a potassium ion with a chloride ion fixed in the reservoir. The two profiles are practically superimposable, with only slight differences of 0.27 and 0.15 kT occurring at the central barrier (at $z = 0$ Å) and the energy wells (at $z = \pm 15$ Å), respectively.

Given that the nanotube is symmetric, the ion positions were sampled only in the positive z domain, and reflected to obtain the negative z PMF. Thus, the ion was moved through positions from 0 to 30 Å in steps of 0.5 Å and the z-component was held using a constraint of 12.5 kcal mol^{-1} Å^{-2}, while the ion was free to move radially. The harmonic constraint was chosen to give adequate overlap between each window while constraining the ion enough to ensure sufficient sampling. The ion's z and r coordinates were obtained during each umbrella sampling run of 1 ns, and runs were analyzed using the weighted histogram analysis method [31,32] to obtain a two-dimensional PMF with the reaction coordinates (z, r). This two-dimensional PMF was then converted thermodynamically into a three-dimensional, radially symmetric PMF.

The free energy profiles and the distribution of frictional and random forces (friction kernel) determined from our MD simulations are then incorporated into stochastic dynamics simulations based on the non-linear generalized Langevin equation, given by

$$\partial_t \mathbf{q}(t) = m^{-1}\mathbf{p}(t),$$
$$\partial_t \mathbf{p}(t) = \mathbf{F_D}(\mathbf{q}(t)) - \int_0^t dt' K(t')\mathbf{p}(t-t') + \mathbf{F_R}(t), \tag{2}$$

where $\mathbf{q}(t)$ and $\mathbf{p}(t)$ are the coordinate and momentum at time t, respectively, m is the mass, $\mathbf{F_D}$ represents the three-dimensional potential of mean force, and the second term represents the frictional force in which $K(t')$ is the friction kernel. The last term, $\mathbf{F_R}$ is the random force which is assumed to be a Gaussian random force related to the friction kernel through the fluctuation–dissipation theorem. This methodology, known as 'distributional molecular dynamics' (DMD) [19], reproduces the distribution of ion trajectories in MD as closely as possible but enables simulations that are 2 to 3 orders of magnitude faster than classical MD simulations. The simulation space is separated into two regions (i) within the pore and (ii) in the reservoir. The pore is divided into thin slices and the forces acting on each ion and the diffusion coefficient are obtained from the three-dimensional PMF and friction kernel determined from MD simulations so that certain properties of the single-ion trajectory are reproduced in DMD. Macroscopic electrostatics is used to determine the ion–ion interaction when two ions are present in the pore. In the reservoir normal Brownian dynamics and macroscopic electrostatics are performed [33]. Using this algorithm, the details of which are given in our previous papers [5,19] we are able to derive macroscopic observables, such as current–voltage–concentration profiles and locations of ion binding sites in the nanotube. The theoretical basis for DMD and a detailed test using gramicidin are given by Gordon et al. [19].

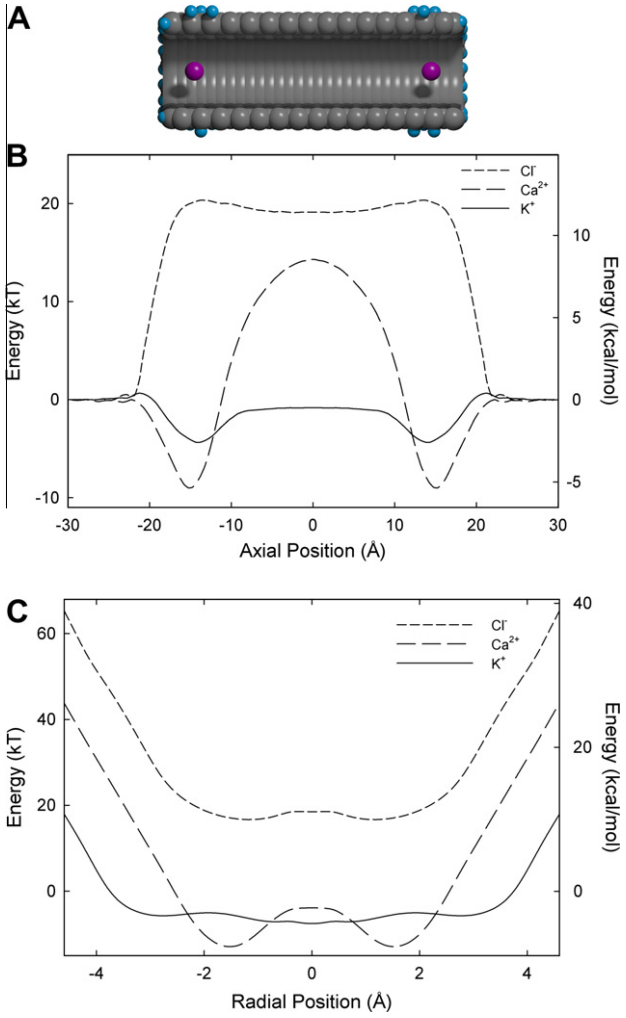

Figure 1. (A) Schematic of the (9,9) CNT with hydrogen terminated ends and exohydrogenated surface (shown in blue). Potassium ions are located at the two binding sites and are shown in pink. (B) Axial and (C) radial free energy profiles of potassium (K^+), chloride (Cl^-) and calcium (Ca^{2+}) ions. The radial free energy profile is taken at $z = 15$ Å.

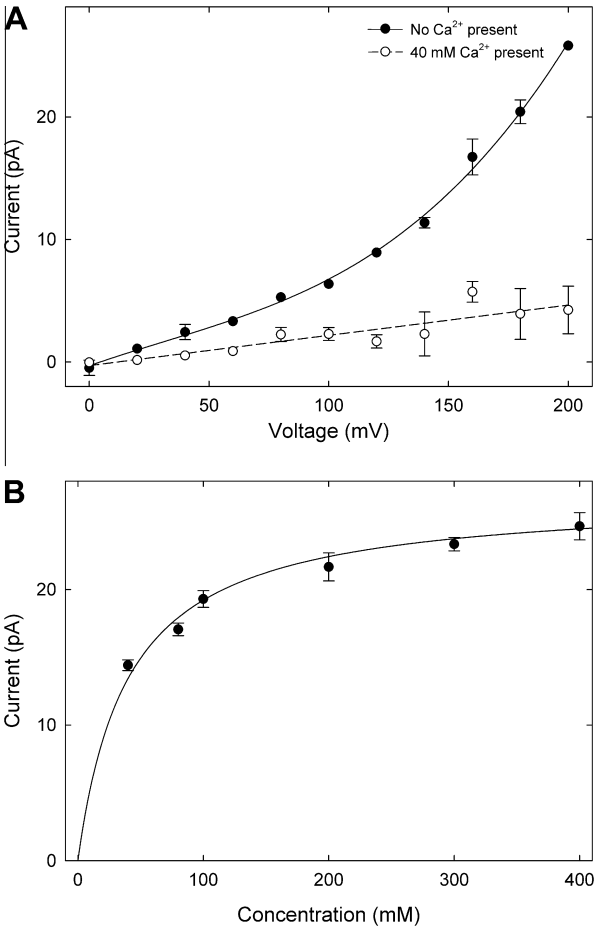

Figure 2. Current–voltage–concentration profiles for potassium ions for the (9,9) exohydrogenated CNT. (A) Current–voltage profile, (B) Current–concentration profile. Each data point represents the average of five sets of simulations, each simulation lasting 0.8 μs. Error bars represent one standard error of the mean and error bars smaller than the data points are not shown.

3. Results and discussion

We construct the profile of free energy encountered by potassium (K^+), chloride (Cl^-) and calcium (Ca^{2+}) ions and then determine frictional and random forces acting on the ions at each discrete segment of the pore [5]. Figure 1B shows the axial free energy profiles of the three ionic species for the (9,9) exohydrogenated CNT which is illustrated in Figure 1A. The free energy profile shown here is derived from the three-dimensional potential of mean force and is therefore the energy the ion encounters as it moves along the axis [5]. For potassium ions, there exist two energy wells of approximately 4.5 kT at either end of the CNT. The minima of the two wells are located at ±15 Å, and are separated by a central barrier of 3.5 kT. This is a similar profile to that seen by a potassium ion in a gramicidin pore determined using Brownian dynamics and the inverse of the available permeation data [34]. Current MD force fields do not predict the correct energy profiles for cations and therefore conflict with experiments [35]. Similarly, for calcium ions there exist two energy wells of 9 kT located at approximately ±15 Å. However, for calcium these wells are separated by an insurmountable energy barrier of 23 kT so that calcium ions are not expected to traverse the channel. Chloride ions are not expected to enter the pore, as they face a steep free energy barrier of approximately 20 kT. The location of these wells aligns with the position of the exohydrogenated regions of the nanotube surface, as illustrated by Figure 1A. Figure 1C shows the radial free energy profiles of the three ionic species taken at an axial position of $z = 15$ Å. As expected the energy increases as the ions approach the nanotube wall. Away from the nanotube wall the energy is relatively flat for potassium and chloride ions. However, for calcium ions there are two distinct energy wells at $r = 1.6$ Å so that calcium would prefer to reside off center.

The current–voltage profile for potassium ions in the (9,9) CNT is shown in Figure 2A. Unlike gramicidin, the current–voltage relationship is non-linear, with a current of approximately 6 pA at 100 mV increasing to 26 pA at 200 mV. This deviation from Ohm's law is a result of the central barrier present for potassium ions (see Figure 1B). The current across this synthetic nanotube is considerably larger than the experimentally measured current across the gramicidin channel [34,36] which has a potassium current of 4 pA at 200 mV and 500 mM. No chloride conductance was observed for all investigated voltages and concentrations.

The current–concentration profile for potassium ions is shown in Figure 2B. Similar to gramicidin, the current saturates with increasing ionic concentration following a Michaelis–Menten form: $I = I_{max}/(1 + K_s/[K])$, where the current I approaches the saturation current I_{max} at 26.9 pA when the concentration $[K]$ is much larger than the concentration at the half saturation point K_s of 40 mM. This half saturation point is much lower than the experimental value of 230 mM at 200 mV for gramicidin [34].

We also examined the influence of calcium ions on potassium conduction using a potassium concentration of 500 mM. The current–voltage profile for potassium ions in the (9,9) CNT with 1 calcium ion present in each reservoir (equivalent to 40 mM calcium concentration) is shown in Figure 2A. By adding 1 calcium ion to each reservoir the potassium current reduces from 26 pA to 4 pA at 200 mV, and adding two calcium ions (data not shown) reduces

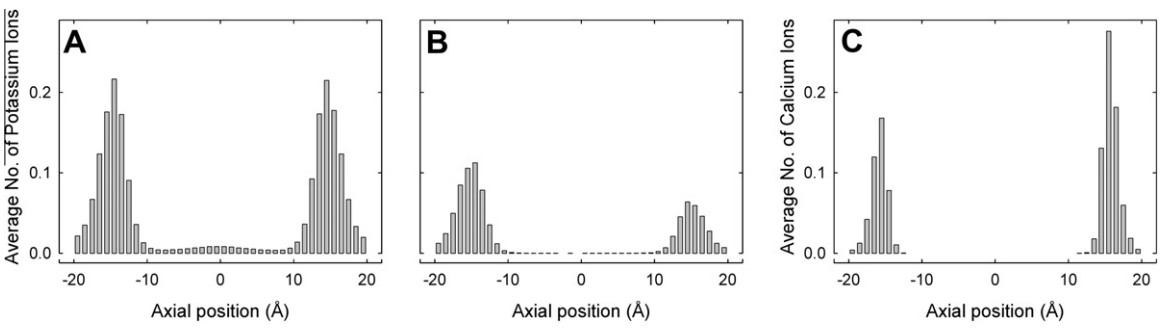

Figure 3. Binding sites in the absence of an applied potential and 500 mM potassium for (A) potassium ions with no calcium present, (B) potassium ions with two calcium ions in each reservoir, and (C) calcium ions with two calcium ions in each reservoir.

the current to 1.6 pA. No calcium ions traverse the nanotube even at calcium concentrations as high as 500 mM.

In the absence of an applied potential, and with no calcium ions present, potassium ions tend to dwell at the location of the two energy wells (at $z = \pm 15$ Å), as shown in Figure 3A. On average there are 0.96 potassium ions in each well. Similarly, in gramicidin [34] there are on average 0.75 ions in each well (located at approximately ± 11 Å). When two calcium ions are added to each reservoir the average number of potassium ions in the entire CNT is reduced from 1.92 to 0.81 (Figure 3B) due to calcium ions blocking the nanotube entrance. Calcium ions tend to dwell at the location of the two energy wells (± 15 Å) with on average 1.13 calcium ions present in the CNT (Figure 3C).

4. Conclusions

We have shown that, in principle, a (9,9) exohydrogenated CNT can broadly mimic the characteristics of the gramicidin-A pore. This synthetic nanotube is selective to monovalent cations, binds divalent cations and rejects anions. In the absence of calcium, the CNT conducts potassium ions six times faster than gramicidin. The tube is normally occupied by two ions, and a conduction event occurs when a third ion enters the pore. Adding 1 calcium ion to each reservoir reduces the potassium current by 85% due to calcium ions binding to the nanotube entrances and blocking the flow of potassium. Chloride ions are rejected from the nanotube in all simulations.

Acknowledgements

We thank Rhys Hawkins from the Visualization Laboratory at the Australian National University and Silvie Ngo for expert graphics preparation. This work was supported by the National Health and Medical Research Council and the MAWA Trust. The calculations upon which this work is based were carried out using the Sun X6275 blades cluster of the Australian National University Supercomputer Facility.

References

[1] A. Kalra, S. Garde, G. Hummer, Proc. Natl. Acad. Sci. USA 100 (2003) 10175.
[2] F. Fornasiero, H.G. Park, J.K. Holt, M. Stadermann, C.P. Grigoropoulos, A. Noy, O. Bakajin, Proc. Natl. Acad. Sci. USA 105 (2008) 17250.
[3] B. Corry, J. Phys. Chem. B 112 (2008) 1427.
[4] T.A. Hilder, D. Gordon, S.H. Chung, Small 5 (2009) 2183.
[5] T.A. Hilder, D. Gordon, S.H. Chung, Biophys. J. 99 (2010) 1734.
[6] S. Joseph, R.J. Mashl, E. Jakobsson, N.R. Aluru, Nano Lett. 3 (2003) 1399.
[7] C.Y. Won, N.R. Aluru, Chem. Phys. Lett. 478 (2009) 185.
[8] T.A. Hilder, D. Gordon, S.H. Chung, Small 5 (2009) 2870.
[9] X. Gong, J. Li, J. Wang, H. Yang, J. Am. Chem. Soc. 132 (2010) 1873.
[10] S. Wang, Z. Liang, B. Wang, C. Zhang, Z. Rahman, Nanotechnology 18 (2007) 055301.
[11] J.L. Bahr, J.M. Tour, J. Mater. Chem. 12 (2002) 1952.
[12] A.R. Hilgenbrink, P.S. Low, J. Pharm. Sci. 94 (2005) 2135.
[13] D. Tasis, N. Tagmatarchis, V. Georgakilas, M. Prato, Chem. Eur. J. 9 (2003) 4000.
[14] C.F. Lopez, S.O. Nielsen, P.B. Moore, M.L. Klein, Proc. Natl. Acad. Sci. USA 101 (2004) 4431.
[15] C.Y. Lee, W. Choi, J.H. Han, M.S. Strano, Science 329 (2010) 1320.
[16] O.S. Andersen, R.E. Koeppe II, B. Roux, Biological Membrane Ion Channels: Dynamics, Structure and Application, Springer, New York, 2007. Ch. Gramicidin channels: versatile tools, p. 33.
[17] M.B. Partenskii, P.C. Jordan, Q. Rev. Biophys. 25 (1992) 477.
[18] S. Kuyucak, O.S. Andersen, S.H. Chung, Rep. Prog. Phys. 64 (2001) 1427.
[19] D. Gordon, V. Krishnamurthy, S.H. Chung, J. Chem. Phys. 131 (2009) 134102.
[20] D. Lu, Y. Li, U. Ravaiolo, K. Schulten, J. Phys. Chem. B 109 (2005) 11461.
[21] A. Nikitin, H. Ogasawara, D. Mann, R. Denecke, Z. Zhang, H. Dai, K.J. Cho, A. Nilson, Phys. Rev. Lett. 95 (2005) 225507.
[22] M.S. Raghuveer, A. Kumar, M.J. Frederick, G.P. Louie, P.G. Ganesan, G. Ramanath, Adv. Mater. 18 (2006) 547.
[23] K.A. Park, K. Seo, Y.H. Lee, J. Phys. Chem. B 109 (2005) 8967.
[24] C.W. Bauschlicher Jr., Nano Lett. 1 (2001) 223.
[25] L. Kalé et al., J. Comput. Phys. 151 (1999) 283.
[26] W. Humphrey, A. Dalke, K. Schulten, J. Mol. Graph. 14 (1996) 33.
[27] B.R. Brooks, R.E. Bruccoleri, B.D. Olafson, D.J. States, S. Swaminathan, M. Karplus, J. Comput. Chem. 4 (1983) 187.
[28] A.D. MacKerell Jr., B. Brooks, C.L. Brooks III, L. Nilsson, B. Roux, Y. Won, M. Karplus, The Encyclopedia of Computational Chemistry, vol. 1, John Wiley and Sons, Chichester, 1998. p. 271.
[29] T. Darden, D. Pearlman, L.G. Pedersen, J. Chem. Phys. 109 (1988) 10921.
[30] M.A. Kastenholz, P.H. Hünenberger, J. Phys. Chem. B 108 (2004) 774.
[31] S. Kumar, J.M. Rosenberg, D. Bouzida, R.H. Swensen, P.A. Kollman, J. Comput. Chem. 16 (1995) 1339.
[32] A. Grossfield, <http://membrane.urmc.rochester.edu/Software/WHAM/WHAM.html> (accessed 20.08.08).
[33] M. Hoyles, S. Kuyucak, S.H. Chung, Phys. Rev. E 58 (1998) 3654.
[34] S. Edwards, B. Corry, S. Kuyucak, S.H. Chung, Biophys. J. 83 (2002) 1348.
[35] T. Baştuğ, S. Kuyucak, Biophys. J. 90 (2006) 3941.
[36] O.S. Andersen, R.E. Koeppe, B. Roux, IEEE Trans. Nanobiosci. 4 (2005) 10.